

A ‘FIREWORK’ OF H₂ KNOTS IN THE PLANETARY NEBULA NGC 7293 (THE HELIX NEBULA) *

M. MATSUURA^{1,2}, A.K. SPECK³, B.M. MCHUNU³, I. TANAKA⁴, N.J. WRIGHT², M.D. SMITH⁵, A.A. ZIJLSTRA⁶, S. VITI², R. WESSON²
ApJ, in press

ABSTRACT

We present a deep and wide field-of-view ($4' \times 7'$) image of the planetary nebula (PN) NGC 7293 (the Helix Nebula) in the $2.12 \mu\text{m}$ H₂ $v = 1 \rightarrow 0$ S(1) line. The excellent seeing ($0.4''$) at the Subaru Telescope, allows the details of cometary knots to be examined. The knots are found at distances of $2.2' - 6.4'$ from the central star (CS). At the inner edge and in the inner ring (up to $4.5'$ from the CS), the knot often show a ‘tadpole’ shape, an elliptical head with a bright crescent inside and a long tail opposite to the CS. In detail, there are variations in the tadpole shapes, such as narrowing tails, widening tails, meandering tails, or multi-peaks within a tail. In the outer ring ($4.5' - 6.4'$ from the CS), the shapes are more fractured, and the tails do not collimate into a single direction. The transition in knot morphology from the inner edge to the outer ring is clearly seen. The number density of knots governs the H₂ surface brightness in the inner ring: H₂ exists only within the knots. Possible mechanisms which contribute to the shaping of the knots are discussed, including photo-ionization and streaming motions. A plausible interpretation of our images is that inner knots are being overrun by a faster wind, but that this has not (yet) reached the outer knots. Based on H₂ formation and destruction rates, H₂ gas can survive in knots from formation during the late asymptotic giant branch (AGB) phase throughout the PN phase. These observations provide new constraints on the formation and evolution of knots, and on the physics of molecular gas embedded within ionized gas.

Subject headings: (ISM:) planetary nebulae : individual (NGC 7293) — ISM: molecules — ISM: globules — infrared: ISM

1. INTRODUCTION

Heterogeneities and filamentary structures in the ionized emission from planetary nebulae (PNe) have been known for many years (e.g. Curtis 1918; Zanstra 1955; Vorontsov-Velyaminov 1968). Such structures are now known to be common in all types of nebulae, including PNe (e.g. Gonçalves et al. 2001; Matsuura et al. 2005; Wesson et al. 2008; Tsamis et al. 2008), star-forming regions (Alves et al. 2001; Thompson et al. 2002) and supernovae (Sugerman et al. 2006). In one of the best studied PNe NGC 7293 (the Helix Nebula), knots in the inner regions have a comet-like shape (e.g. Zanstra 1955; Meaburn et al. 1992; O’Dell & Handron 1996) and are thus known as cometary knots. Their apparent ubiquity in PNe has led to the assertion that all circumstellar nebulae are clumpy in structure (O’Dell et al. 2002; Meixner et al. 2005). Understanding their physical nature, such as line excitation and formation mechanism, is essential to understanding the dominant physics governing nebulae.

In order to discuss the nature and origin of the density inhomogeneities and their manifestation in PNe, we first need to define our terminology. The term “cometary knot” is used to refer to structures that include both an elliptical head and a trailing tail (although both these structures come in a variety of shapes). Consequently we define “knot” to mean the whole “cometary” structure (head and tail, if a tail exists on a given knot-head). These structures are sometimes referred to as globules, but we prefer to use the term “globule” to refer to the head only (and in some cases there is only a head, in which case it is both a knot and a globule). In addition to knots, various previous work on small-scale inhomogeneities have also defined FLIERS (Fast Low-ionization Emission Regions; Balick et al. 1998) and LIS (low-ionization structures; Gonçalves et al. 2001). Knots are a subset of LIS, but not of FLIERS (too slow). In terms of the formation and shaping of knots, we also define the term “core”, which is taken to be a density enhancement in the nebula which is subsequently molded by some mechanism into a knot.

We have obtained a new high resolution H₂ image of the Helix Nebula using MOIRCS (Multi-Object Infrared Camera and Spectrograph; Ichikawa et al. 2006) on the 8.2-meter telescope, Subaru. Two slightly elongated ellipses (Fig. 1) of NGC 7293 are interpreted as projected rings: an inner ring (from about $200''$ up to $500''$) and an outer ring (up to $740''$)⁸. Inside the inner ring, i.e., the inner edge, isolated knots have been found (e.g. O’Dell & Handron 1996). The MOIRCS wide field of

* Based on data taken with the Subaru Telescope, National Astronomical Observatory of Japan (proposal ID S07B-054)

¹ National Astronomical Observatory of Japan, Osawa 2-21-1, Mitaka, Tokyo 181-8588, Japan; e-mail: m.matsuura@nao.ac.jp

² Department of Physics and Astronomy, University College London, Gower Street, London WC1E 6BT, UK; e-mail (m.m.): mikako@star.ucl.ac.uk

³ Physics and Astronomy, University of Missouri, Columbia, MO 65211, USA

⁴ Subaru Telescope, National Astronomical Observatory of Japan, 650 North Aohoku Place, Hilo, HI 96720, USA

⁵ Centre for Astrophysics and Planetary Science, University of Kent, Canterbury CT2 7NH, UK

⁶ Jodrell Bank Centre for Astrophysics, University of Manchester, Oxford Street, Manchester M13 9PL, UK

⁸ Note that this is only a description of the nebula’s appearance on the sky, and is not intended to denote its 3-d structure (c.f. O’Dell et al. 2004)

view (FOV; $4' \times 7'$) yields an image covering the inner and outer rings as well as the central star (CS) as indicated in Fig. 1. The excellent seeing ($\sim 0.4''$ in FWHM; full width at half maximum) allows resolution of the individual knots (typically $1\text{--}3''$ in diameter). Combining the large FOV and high spatial resolution, we are able to study the radial variation of knot shapes and number densities.

2. OBSERVATIONS AND DATA-REDUCTION

Infrared images of NGC 7293 were taken with the MOIRCS on the Subaru Telescope at Mauna Kea, Hawaii, USA on 2007 June 25 (UT) during the twilight. The sky condition was photometric. We used telescope nodding to 1° to the east to subtract the sky background. Jitter was used to minimize the influence of hot pixels. The total exposure time was $100\text{s} \times 7$ on source. Telescope ambient seeing in the optical was $0.5''$ and the spatial resolution of the reduced image is measured as $\sim 0.4''$ (FWHM), measured by stars within the field. The airmass during the observations was 1.3. MOIRCS is installed with two 2028×2028 pixel HAWAII-2 arrays, namely CH1 and CH2, and pixel scale is $0.117''$. The H_2 filter has a central wavelength of $2.116\ \mu\text{m}$ and a width of $0.021\ \mu\text{m}$ (FWHM). Continuum emission from the nebula is probably negligible at this wavelength (Matsuura et al. 2007) at least at the inner edge, and the $\text{H}_2\ v = 1 \rightarrow 0\ \text{S}(1)$ line is dominant. The coordinates of the center of the final image are RA= $22\text{h}29\text{m}43.02\text{s}$, DEC= $-20\text{d}47\text{m}33.3\text{s}$ (J2000) and the position angle is 25.4° east of north. The MOIRCS observed region is indicated on Hora et al. (2006)'s Spitzer image (Fig. 1), which shows the general location of the inner and outer rings and the inner edge of NGC 7293. The MOIRCS image covers the CS and part of both of these two rings.

Our Helix image has an angular resolution comparable to previous HST NICMOS images (Meixner et al. 2005; O'Dell et al. 2007). The pixel scale of NICMOS NIC3 camera is $0.2''$, the Nyquist sampling provides a resolution (FWHM) of $0.4''$. Meixner et al. (2005) and O'Dell et al. (2007) have taken two frames at each field with slightly different positions to increase the spatial sampling. Depending on the pointing accuracy, the final images combining two different positions would create a spatial resolution of $0.2\text{--}0.4''$. Indeed, O'Dell et al. (2007) reported the FWHM of a star of $0.42''$. We measured FWHMs of two stars in two different fields in Meixner et al. (2005), yielding $0.20\text{--}0.42''$. Our MOIRCS ($0.4''$) image is among the highest angular resolution images of multiple knots of the Helix at $2\ \mu\text{m}$, after the observations of a single knot at $0.05''$ pixel scale of Matsuura et al. (2007).

We use *IRAF* and the *IRAF*-based software *QMCS* which has been developed by one of the authors (I.T.) for the data reduction. We first adopted the correction of the flat field, the sky subtraction and the distortion correction, and a mosaic image was created from seven target frames by registering field stars and by adopting masks on bad pixels. In the final image, there are low level artifacts in the form of multiple circular rings on the image taken with one of the arrays. This pattern is caused by interference of the filter. In the CH1 image (the south part of the image), this pattern was reduced using `defringe_moircs.pro`, which is a part of 'SIMPLE Imag-

ing and Mosaicing Pipeline' (Wang, in preparation). The sensitivity is approximately $3 \times 10^{-19}\ \text{ergs s}^{-1}\ \text{cm}^{-2}\ \text{\AA}^{-1}$ at a signal-to-noise ratio of 5. The RMS noise on the sky level was measured over five hundreds circular apertures (radius of $0.39''$; approximately twice the FWHM of the seeing limit) on the blank space of the CH1 image. The median of the RMS noise distribution is taken as the sensitivity. We use 2MASS magnitudes of three stars in CH1, and we assume that their *K*s magnitudes are identical in the H2 filter. No such measurement is possible in CH2, because of the high density of knots. A similar measurement is applied to NICMOS images (Meixner et al. 2005), giving $3 \times 10^{-18}\ \text{ergs s}^{-1}\ \text{cm}^{-2}\ \text{\AA}^{-1}$. The sensitivity of our MOIRCS image is better than the NICMOS images by an order of magnitude.

3. RESULTS

3.1. Overall descriptions of the H_2 image

Fig. 2 shows the MOIRCS image of NGC 7293 in the $v \rightarrow 1\text{--}0\ \text{S}(1)\ \text{H}_2$ line, while Fig. 3 shows a grid reference indicating the R.A. and Dec. (J2000) overlaid on the image, together with a numbered grid to guide the reader to which region we are discussing. Clumps of H_2 gas are found throughout the entire image (except the area close to the central star), supporting Meixner et al. (2005) and Hora et al. (2006). The knots are isolated at the inner edge (distance from the CS $r < 3.5'$) and these knots are accompanied by tails pointing directly away from the CS. The areas enlarged in Fig. 4 are indicated in Fig. 3. Individual knots and their tails remain resolved throughout the inner ring ($3.5' < r < 4.5'$). While the H_2 emission is clumpy in the outer ring ($4.5' < r < 6.4'$), the structures are different; individual knots are not as easy to distinguish, and tails do not appear to be collimated into the radial direction (Fig. 4). The outer ring is brighter than the inner ring in H_2 , as found by Speck et al. (2002). Our MOIRCS image clearly shows that the morphology of the knots changes from the inner edge to the outer ring. In general, the well-resolved knots in the inner edge and inner ring show a 'cometary' shape, i.e. an elliptical head including a bright crescent-shaped tip and a tail. In the inner region, the crescents always face the CS, and the tails stretch in the opposite direction. Examples of morphologies are found in Figs. 4 and 5. Such knots are found up to $r \sim 4.5'$ (approximately the lower half of Fig. 2) from the CS, i.e., the inner ring. From previous observations, the cometary morphology has only been recognized at the inner edge (Huggins et al. 2002; Hora et al. 2006; Matsuura et al. 2007). Our MOIRCS image shows that these morphologies are found throughout the inner ring.

Beyond $r \sim 4.5'$ (the outer ring), tails are not always obvious; some knots appears to have crescents only (Fig. 4), as described by Meixner et al. (2005) and O'Dell et al. (2007).

3.2. Detailed descriptions of tails

The shapes of the tails are best studied in H_2 due to its brightness. Matsuura et al. (2007) studied a knot at the inner edge of the H_2 emitting region and showed that the optical [NII] + $\text{H}\alpha$ intensity falls to less than 10% at $1''$ away from the brightest tip, while the H_2 intensity decreases more gradually to 10% at $5''$.

Fig. 5 displays a variety in tail shapes. The knots in this figure are mostly located in the inner edge (Fig. 3) and they are well isolated. The most common shape is a narrowing tail, which was also found for an individual knot at the highest angular resolution (0.05'' per pixel) (Matsuura et al. 2007, 2008). However, some tails first narrow then widen with distance from the bright tip, such as knot (h) in Fig. 5. Similarly, some tails show a brightness gap at the midpoint along the tail (d) and (e). Such tail shapes have not been reported previously. There is one case of a continuously widening tail straight from the crescent (g). Knots occasionally show complex structures, with a secondary peak or sometimes multiple intensity peaks in the tail, often accompanied by a meandering tail (a), (c), and (f). The orientation of the tail often changes at the secondary peak (a) and (f). As the secondary peak is aligned with the tail, and no crescent is found nearby, the secondary peak is physically associated with the primary peak. The wide variety of tails may be linked with the formation mechanisms of knots and tails, or they trace an interaction with the local environment. This will be discussed in Sect. 4.3.

3.3. Number density of knots and H₂ surface brightness

We counted the number density of knots and compared with the H₂ surface brightness. Fig. 6 shows the number of knots counted in 1×1 arcmin² regions, as a function of average surface brightness within these regions calculated from Speck et al. (2002). In the inner ring, the surface brightness of H₂ correlates well with the number density of H₂ knots, rather than with the brightness of individual knots, or the distance from the CS.

For a similar number density of knots, the outer ring has twice as high surface brightness as does the inner ring. This is due to a contribution from blended H₂ tails, which occupy a larger area than the knot-heads in the outer ring, as found in Figs. 2 and 4. On average, the H₂ surface brightness from the outer ring is higher than that from the inner ring.

In order to estimate the total number of knots in this nebula, we divide the nebula into three zones, the innermost edge ($r=2.2-3.5'$), the inner ring ($r=3.5-4.5'$) and the outer ring ($r=4.5-6.4'$). From the MOIRCS image, we estimate the knot number densities of these regions to be 20, 500 and 400 arcmin⁻², respectively. We assume that knots are uniformly distributed in these circular rings. The total number of knots is estimated to be 4×10^4 in the entire nebula. This is a factor of 1.7 larger than the estimate by Meixner et al. (2005). The difference is caused by the assumed knot number densities in the inner ring; Meixner et al. (2005) used a lower number density (148 arcmin⁻²) throughout the entire nebula based on observations of the outer ring. We counted knot number densities in relatively less crowded regions within our image so as to minimize confusion problems. Despite that, these regions are bright in the Spitzer 3.6 μ m image, where the 3.6 μ m band also represents H₂ emission (Fig. 1; Hora et al. 2006). Meixner et al. (2005) counted much fainter regions, where the density is lower. The total number of knots provides an estimate of the total molecular and neutral hydrogen gas mass. Adopting a knot mass of $1.5 \times 10^{-5} M_{\odot}$ (O'Dell & Handron 1996), the total molecular mass is $0.6 M_{\odot}$ in this nebula. This estimate is a factor six larger than the molecular mass es-

timated from CO observations (Young et al. 1999). The difference could be due to the large fluctuations of knot mass. Since the ionized gas mass is estimated as $0.3 M_{\odot}$ in this nebula (Henry et al. 1999), a substantial amount of molecular gas remains. Most of the H₂ gas is found in the outer ring, thus the distance from the CS, i.e. UV radiation strength is a key. Only knots with large optical depth could survive in the inner ring.

3.4. Comparisons with optical images

NGC 7293 has been targeted by various optical observations. Figs. 7, 8 and 9 shows a comparison of the MOIRCS H₂ image with HST images in the F658N and F656N filters (O'Dell et al. 2005; O'Dell & Handron 1996, respectively). The F656N data at 656 nm are dominated by H α with some contamination from [NII], whereas the F658N data at 658 nm are dominated by [NII], with negligible contamination from H α . The F656N image has been taken only for smaller parts of the Helix Nebula.

Fig. 7 shows the overall images of H₂ and F658N. The brightest places in H₂ and [NII] are found in different locations within the nebula. The inner ring is brighter than the outer ring in [NII] whereas the outer ring is brighter in H₂. All knots in the optical image have counterparts in H₂ emission. Some knots cause extinction in the optical (and appear dark in the image), as found near the bottom of the [NII] image (Fig. 7). These knots are located in the foreground of diffuse ionized emission, and all of these absorption knots in [NII] have emission counterparts in the H₂ image (c.f. the case of NGC 6720; Speck et al. 2003). In contrast, not all H₂ knots have corresponding knots in the [NII] image, particularly in the inner ring where [NII], emission from the inter-knot region overwhelms the emission from knots, if any. Meixner et al. (2005) and O'Dell et al. (2007) suggested that H₂ knots always have some counterparts in [NII] but this is only the case in the outer ring and at the inner edge. In the outer ring, diffuse [NII] components are relatively weak, and in the inner edge, all of the knots are isolated. This contrast can be explained if NGC 7293 takes the morphology of a pole-on bipolar nebula projected onto two rings (O'Dell et al. 2004; Meaburn et al. 2005). Moreover, these rings are quite thick and contain layers of knots and diffuse components within.

Fig. 8 shows a close-up comparison of the H₂, [NII] and H α images in the inner ring, labeled as regions 5 and 6 in Fig. 3. The F656N image is available only for region 6 within the MOIRCS 13 regions defined in Fig. 3. Knots are clearly found in the H₂ images for both regions 5 and 6, whereas less than one-third of those crescents/heads are recognised in [NII] image. In the [NII] images, there is little to no structure defining the knots, with the ionized emission being more diffuse. In region 6, the H₂ crescents have counterparts in H α , except where indicated by arrows in Fig. 8.

H₂ is associated only with high density knots, whereas the ionized gas is located both at the surface of the knots and in the inter-knot space. The high density of the knots leads to high brightness in the knot locations for H₂ and to a lesser extent, H α . The H α contrast is reduced by the inter-knot component.

We further compare H₂, [NII] and H α images of well-isolated knots in the inner edge of the nebula (Fig. 9).

These images are aligned such that the tips of the knots are coincident at these three wavelength. O'Dell et al. (2005) reported a displacement of the [NII] tips with respect to those in NICMOS H α and H $_2$ by $\sim 0.1''$: this displacement is minor compared to our $0.4''$ resolution. All knots except (b) were detected in [NII], but only three were found in H α . All crescents are found in all three wavelengths. The secondary peaks in knots (a), (c), and (f) are also found in all wavelength images: fainter local peaks in the H $_2$ image of knot (f) can be seen in the H α image, but not in the [NII] image. In the [NII] and H α images, high emission from the inter-knot region is found. Due to this high inter-knot emission and faintness of tail emission, the narrowing of the tails is not always clearly seen in the [NII] image.

4. DISCUSSION

4.1. Origin of the molecular hydrogen in knots

Our observations show that at the inner edge and the adjacent regions of the nebula, the H $_2$ is found only in knots. In the outer ring there is a faint dispersed H $_2$ component which can be interpreted as overlapping blended tails. Therefore, we conclude that the H $_2$ is associated solely with the knots, following Speck et al. (2002) and Meixner et al. (2005). There are two plausible explanations for such an association: (i) the large optical depth of the knots protects previously formed H $_2$ from the harsh UV radiation, or (ii) the H $_2$ formed in-situ in the knots, where high densities and low temperatures allow for molecule formation.

The choice between these two explanations is linked to the origin of the knots: did these form at late times, after ionization of the planetary nebulae began (e.g. Garcia-Segura et al. 2006), or did they originate in a molecular wind (e.g. Redman et al. 2003)? In the first case, H $_2$ must have formed in-situ, while in the second case the molecular content may have survived from the AGB wind.

In order to test whether H $_2$ formed during the AGB phase could have survived into the PN phase, we have investigated the lifetime of molecular hydrogen. Using the dissociation rate of H $_2$, including self-shielding (Draine & Bertoldi 1996) and $G_0 = 8$ and $n_{\text{H}_2} = 8 \times 10^4 \text{ cm}^{-3}$ (Matsuura et al. 2007), the time scale to dissociate H $_2$ is estimated to be 8×10^7 years. Thus, pre-existing H $_2$ can survive in dense regions within the current conditions. However, the UV radiation field will have been much stronger in the past. The star is currently on the cooling track, and is much less luminous than during its earlier post-AGB evolution. If $G_0 = 10^3$, the dissociation time scale is 8×10^4 years. The high-luminosity regime phase for relatively massive stars lasts for less than 10,000 yrs (Zijlstra et al. 2008). Hence, the H $_2$ associated with knots may have survived such an intense UV radiation field for this early post-AGB period.

In order to investigate whether H $_2$ can be formed in-situ in PNe, Aleman & Gruenwald (2004) calculated H $_2$ formation in (partly) ionised gas. The reactions involved include $\text{H}^- + \text{H}$ and $\text{H}_2^+ + \text{H}$. The H $_2$ formation rate in the ionized gas is estimated to be $10^{-10.5} \text{ cm}^{-3} \text{ s}^{-1}$ in total, which is slightly larger than the H $_2$ destruction rate. However, the fraction of H $_2$ with respect to H is extremely small (10^{-5}). Aleman & Gruenwald (2004) con-

cluded that some H $_2$ could survive the ionized state, but it is not yet clear if H $_2$ can be formed from the ionized gas during the PN phase.

The densities within the knots are estimated to be 10^6 cm^{-3} (Meaburn et al. 1998) to $3 \times 10^5 \text{ cm}^{-3}$ (Huggins et al. 2002). At 10^6 cm^{-3} , H $_2$ formation on dust grains becomes significant; the time scale is of the order of 10^3 yr. Thus, in the densest knots the formation can proceed faster than the age of the nebula. However, if the densities are lower, the required life time of the knots becomes similar to the age of the nebula. In such a case, the knots pre-date the ionization, removing the need to (re-)form the H $_2$ later.

In summary, the time scale suggest that part of the H $_2$ is primordial, i.e. formed during the AGB phase, and survived the ionization of the nebula. In dense knots, (re-)formation of H $_2$ is possible.

4.2. Knot formation models

There have been various suggested mechanisms for knot formation. The two main scenarios are: (1) the knots are primordial density enhancements, i.e. they started their formation during the AGB phase (e.g. Zanstra 1955; Dyson et al. 1989; Soker 1998)⁹; (2) the knots form in situ, as a result of the onset of the PN phase (e.g. Garcia-Segura et al. 2006; Capriotti 1971).

The in-situ formation mechanisms can be further divided into subcategories: (i) turbulent (Rayleigh-Taylor; RT) instabilities as a result of interaction between the slow and fast winds (e.g. Mathews 1969; Vishniac 1994; Dwarkadas & Balick 1998; Garcia-Segura et al. 2006); (ii) turbulent (Rayleigh-Taylor; RT) instabilities at the ionization front (e.g. Capriotti 1971); (iii) shadowing effects (e.g. Van Blerkom & Arny 1972; Soker 1998); and (iv) radiative shocks (e.g. Walder & Folini 1998). Capriotti (1973) used his model to predict the mass ($10^{-6} M_{\odot}$) and number of knots ($\sim 10^5$) in a nebula, consistent with current observations.

A pre-ionization origin of the knots appears to be plausible. The system of knots has an expansion velocity which is typical for AGB winds but is less than that of the ionized gas (Meaburn et al. 1998). The last point suggests that the knots formed after the AGB wind reached its terminal velocity (at ~ 10 AU from the star), but before the overpressure from the onset of ionization caused further acceleration (e.g. Ueta et al. 2006). The fact that a very high fraction of the total mass is found in the knots, also is more easily reconciled with an early origin.

To form knots in an expanding wind requires compression of the gas, within an overpressured (heated) surrounding region. This may happen at the ionization front, as discussed above. Because the ionization front moves outward, the inner sets of knots would be older than the outer knots, in this model. The shock front between the fast and slow wind is another option but this front co-moves with the expanding nebula, so that one might expect the knots to be found only near the inner edge of the dense nebula. This interface is located within the ionized region, so that one may expect the knots to share the velocity with the ionized gas. This

⁹ At the time of Zanstra (1955), the AGB phase was not established yet, but we count that the phase before gas ionization mean AGB phase and possibly post-AGB phase

model cannot be entirely excluded but may be less in agreement with the observations. In this case, the H₂ would have to form from ionized gas. In either of these cases, the knots would be a very common phenomenon in planetary nebulae.

To form the knots much earlier, in the AGB wind, would require a denser region than normally expected in AGB winds. However, if the AGB star has a close binary companion, a spiral shock will form in the AGB wind behind the companion (Edgar et al. 2008). This shock causes a heated, compressed region, which a large fraction of the AGB ejecta pass through. This could provide a possible location for the origin of the knots. In the absence of detailed hydrodynamical models, this must remain speculative. In this model, the outer knots are older than the inner knots.

4.3. *Shaping knots and tails*

The problem of distinguishing between formation mechanisms becomes even more difficult once we consider the shaping of the knot heads and tails. Most recent studies of knot shapes assume a pre-existing density enhancement and do not consider whether it is primordial or formed during the PN phase. Consequently, observations of knot (head and tail) shapes, may be able to distinguish between shaping models, but are unlikely to reveal the origin of the original density enhancement.

The shaping mechanisms can be also classified into three basic categories, with some cross-fertilization: (a) Hydrodynamic interaction between winds and density enhancements (e.g. Zanstra 1955; Vishniac 1994; Pittard et al. 2005; Dyson et al. 2006; Pittard et al. 2008); (b) Interaction (including photoevaporation) of material with ionizing (UV) radiation (e.g. Mellema et al. 1998; Williams 2003; Garcia-Segura et al. 2006; López-Martín et al. 2001); (c) The effect of shadowing by density enhancements (e.g. Soker 1998; Cantó et al. 1998). These mechanisms may act together, and disentangling which mechanisms are mutually consistent and which are mutually inconsistent is a challenge.

In the following, we will first discuss streaming models, followed by photo-evaporation and shadowing models. A combination is proposed based on the observational constraints.

In all cases discuss below we use the term “core” to describe the density enhancement which is acted upon by the various mechanisms to create cometary knot shapes (heads and tails).

The first proposed mechanism was the interaction of a core with a wind (which may emanate from the CS or be caused by expansion of the inter-knot gas; Zanstra 1955). This basic concept was also the inspiration for Dwarkadas & Balick (1998), who showed that by including an evolution in the fast wind, small clumpy structures could be formed, but the resulting shapes are not described. A more recent attempt to modify this concept includes both an ambient wind, which can be sub- or supersonic, and a flow from the core itself, where flow is assumed to have a constant ablation. We call this a ‘stream’ model. The wind is due to the differential velocity between the diffuse gas and the knots: there is no evidence for a hot wind from the central star.

The interaction between the core and the wind can

create both the heads and the tails (Pittard et al. 2005; Dyson et al. 2006). In this model, the crescent tip is a bow-shock (ignoring photo-ionization) and ram pressure creates a narrowing tail for subsonic ambient winds (Pittard et al. 2005) and a widening tail for supersonic ambient winds.

The second option, i.e. interaction of material with ionizing (UV) radiation, considers photo-ionization and photo-evaporation models, ignoring streaming motions (e.g. Mellema et al. 1998; Garcia-Segura et al. 2006; López-Martín et al. 2001). In this case, the surface of a core facing the CS is illuminated by UV radiation, which causes heating and photo-evaporation from the core, and creates the crescent tip. At this moment, there is no detailed hydrodynamical model present to reproduce narrowing, widening and meandering tails, using photo-evaporation. Williams (2003) calculated ionization front instabilities, and obtained a jet shape. No clear resemblance is found yet between the modelled shape and the knots observed in the Helix Nebula, however, the explored parameter space was limited.

The final possibility is the shadowing by density enhancement (Cantó et al. 1998), leading to non-ionized regions in the shadow. Here, the knots can trace a large core, consisting of neutral gas and dust, with a bright sunny side and a dark shadow giving rise to the tail. UV photons from the CS do not reach the shadowed side directly, but diffuse UV radiation diffusion illuminates the tail. To explain narrowing tail (Cantó et al. 1998) and widening tail (O’Dell et al. 2005), varying angles of illumination are used.

The tails can be explained either with streaming motion, by interaction at the ionization front or by shadowing. Here the streaming models or ionization models appear better able to fit the available data. The bright (and well-isolated) inner knot located in our field, shows clear acceleration in [N II] along the tail (Meaburn et al. 1998), by about 10 km s^{-1} . The meandering tails are consistent with instabilities expected for streaming motions (e.g. Wareing et al. 2007) or interaction at ionization front (Williams 2003), whilst solely shadowing by density enhancement requires straight tails by necessity. (In some case ionization edges are visible within the tails.) Finally, the absence of clear tails in the outer regions is less easily explained with shadowing. The issue is controversial, and further velocity information would be required to resolve it.

As mentioned before, the knots change appreciably in appearance between the inner and outer nebula. In the inner nebula, tails are always seen. In the outer nebula, the knots appear more diffuse and tails are absent. This implies a change in shaping mechanism. Whereas streaming motions appear important in the inner region, the structures in the outer nebula suggest that it does not play a role there. Within the streaming model, the implication is that the knots have a differential velocity with respect to the ambient medium in the inner nebula, but not or less so in the outer nebula. A plausible model is that the inner knots system is being overrun by faster expanding, lower density gas, but that this has not yet reached the outer knot system.

Meaburn et al. (1998) find a difference in expansion velocity between the system of knots and the ionized gas,

of 17 km s^{-1} , with the knots moving slower. The wind speed in the nebula shows significant variations, with velocities up to 50 km s^{-1} with respect to the nebula mean velocity (Walsh & Meaburn 1987). The sound speed in the ionized nebula is of the order of 10 km s^{-1} . This is similar to the velocity differential: we may expect both sub-sonic and super-sonic winds, depending on the local conditions and on the flow velocity within the tail.

If the gas flow models are correct, it points to the prevalent wind interaction being subsonic, because of the common presence of narrowing tails. However, there are also cases of widening tails (knot f), which requires supersonic winds. It would be of interest to measure detailed velocity fields for the tails and the surrounding gas. The tail velocities may possibly be measured from the H_2 lines.

Some of the more complicated tail structures may be due to feedback, where an ambient wind is disturbed by another knot. The multiple brightness-peaks and meandering tail in a knot (Fig.5) may be explained through the complex interaction between nearby cores (Pittard et al. 2005).

Fig. 5 shows that some knots have a dip in brightness in the middle of the tail which remains unexplained. If this is due to the pressure balance, the temperature would be lowest at this point and increase again further out (related to the shadowing by the knot). It could also be due to a change to a supersonic flow at this point (Pittard et al. 2008). Detailed studies of temperature and velocity distribution along these tails may help distinguish the various models, in so far as possible.

It does not appear possible to view the three models in isolation. In reality, a combination of effects is likely required. Streaming motions can help explain the shapes, but the observed structures implies that streaming motions only occur in the inner nebula, not the outer. The crescent shapes trace photo-ionization, and photo-evaporation. Shadowing will occur, but its importance to the shaping remains to be proven. Integrated models taken all effects into account would be desirable.

5. CONCLUSIONS

We have obtained a wide field view image of the Helix nebula in excellent seeing conditions. Knots are found throughout the inner edge to the outer ring, and H_2 is always associated with knots. Chemical and PDR models do not favour H_2 formation in the ionized and neutral gas in planetary nebulae, suggesting that the observed H_2 gas is a remnant of molecular gas formed during the AGB phase. The MOIRCS image shows that knots come in a variety of shapes. These various knot morphologies suggest that the inner knots are being overrun, and shaped by, a faster wind. However, such a wind would not yet have reached the outer system of knots,.

We appreciate technical support from the Subaru Telescope staff during the observations. M.M. is a JSPS fellow. M.M. appreciates discussions at UCL. We also thank for Dr. J.M. Pittard for detailed explanations about his model.

Facilities: Subaru Telescope, MOIRCS

REFERENCES

- Aleman, I., & Gruenwald, R., 2004, ApJ, 607, 865
 Alves, J.F., Lada, C.J., Lada, E.A., 2001, Nature 409, 159
 Balick, B., Alexander, J.H., Arsen, R., Terzian, Y., Perinotto, M., Patriarchi, P., 1998, AJ 116, 360
 Bell, T.A., Viti, S., Williams, D.A., Crawford, I.A., Price, R.J., 2005, MNRAS 357, 961
 Cantó, J., Raga, A., Steffen, W., Shapiro, P., 1998, ApJ 502, 695
 Capriotti, E., 1971, ApJ 166, 563
 Capriotti, E., 1973, ApJ 179, 495
 Cardelli, J.A., Clayton, G.C., Mathis, J.S., 1989, ApJ 345, 245
 Curtis, H.D., 1918, Publication of Lick Observatory, 13, 55
 Draine, B.T., Bertoldi, F., 1996, ApJ 468, 269
 Dwarkadas, V.V., & Balick B., 1998, ApJ 497, 267
 Dyson, J.E., Hartquist, T.W., Pettini, M., Smith, L.J., 1989, MNRAS 241, 625
 Dyson, J.E., Pittard, J.M., Meaburn, J., Falle, S.A.E.G., 2006, A&A 457, 561
 Edgar, R.G., Nordhaus, J., Blackman, E.G., & Frank, A., 2008, ApJ, 675, L101
 García-Segura, G., López, J.A., Steffen, W., Meaburn, J., Manchado, A., 2006, ApJ 646, L61
 Gonçalves D.R., Corradi, R.L.M., Mampaso, A., 2001, ApJ 547, 302
 Harris, H.C., et al. 2007, AJ, 133, 631
 Henry, R.B.C., Kwitter, K.B., Dufour, R.J., 1999, ApJ 517, 782
 Hora, J.L., Latter, W.B., Smith, H.A., Marengo, M., 2006, ApJ 652, 426
 Huggins, P.J., Forveille, T., Bachiller, R., Cox, P., Ageorges, N., Walsh, J.R., 2002, ApJ 573, L55
 Ichikawa, T., et al. 2006, SPIE, 6269, 38
 López-Martín, L., Raga, A.C., Mellema, G., Henney, W.J., Cantó, J., 2001, ApJ 548, 288
 Mathews, W., 1969, ApJ, 157, 583
 Matsuura, M., et al., 2005, MNRAS 359, 383
 Matsuura, M., et al., 2007, MNRAS 382, 1447
 Matsuura, M., et al., 2008, ESO Messenger 132, 37
 Meaburn, J., Walsh, J.R., Clegg, R.E.S., Walton, N.A., Taylor, D., Berry, D.S., 1992, MNRAS 255, 177
 Meaburn, J., et al., 1998, MNRAS 294, 201
 Meaburn, J., et al., 2005, MNRAS 360, 963
 Meixner, M., McCullough, P., Hartman, J., Son, M., Speck, A., 2005, AJ 130, 1784
 Mellema, G., Raga, A.C., Canto, J., Lundqvist, P., Balick, B., Steffen, W., Noriega-Crespo, A., 1998, A&A 331, 335
 Natta, A., Hollenbach, D., 1998, A&A 337, 517
 O'Dell, C.R., Handron, K.D., 1996, AJ 111, 1630
 O'Dell, C.R., Balick, B., Hajian, A.R., Henney, W.J., & Burkert, A., 2002, AJ, 123, 3329
 O'Dell, C.R., McCullough, P.R., Meixner, M., 2004, AJ 128, 2339
 O'Dell, C.R., Henney, W.J., Ferland, G.J., 2005, AJ, 130, 172
 O'Dell, C.R., Henney, W.J., Ferland, G.J., 2007, AJ, 133, 2343
 Pittard, J.M., Dyson, J.E., Falle, S.A.E.G., Hartquist, T.W., 2005, MNRAS 361, 1077
 Pittard, J.M., Falle, S.A.E.G., Hartquist, T.W., Dyson, J.E., 2008, MNRAS, in press, (arXiv0807.4402)
 Redman, M.P., Viti, S., Cau, P., & Williams, D.A., 2003, MNRAS, 345, 1291
 Soker, N., 1998, MNRAS 299, 562
 Speck, A.K., Meixner, M., Fong, D., McCullough, P.R., Moser, D.E., Ueta, T., 2002, AJ 123, 346
 Speck, A.K., Meixner, M., Jacoby, G.H., Knezek, P.M., 2003, PASP 115, 170
 Sugerman, B., et al., 2006, Sci 313, 196
 Thompson, R.I., Smith, B.A., Hester, J.J., 2002, ApJ 570, 749
 Tsamis, Y.G., Walsh, J.R., Péquignot, D., Barlow, M.J., Danziger, I.J., Liu, X.-W., 2008, MNRAS 386, 22
 Ueta, T., Speck, A.K., Stencel, R.E. et al., 2006, ApJ 648, L39
 van Blerkom, D., & Arny, T.T., 1972, MNRAS 156, 91
 Vishniac, E.T., 1994, ApJ 428, 186
 Vorontsov-Velyaminov, B.A., 1968, IAUS 34, 256
 Walder, R., & Folini, D., 1998, A&A 330, L21
 Walsh, J.R., Meaburn, J., 1987, MNRAS 224, 885

- Wareing, C.J., Zijlstra, A.A., O'Brien, T.J., 2007, MNRAS 382, 1233
- Wesson, R., Barlow, M.J., Liu, X.-W., Storey, P.J., Ercolano, B., de Marco, O., 2008, MNRAS 383, 1639
- Williams, R.J.R., 2003, RMxAC 15, 184
- Young, K., Cox, P., Huggins, P.J., Forveille, T., Bachiller, R., 1999, ApJ 522, 387
- Zanstra, H., 1955, Vistas in Astronomy, vol. 1, Issue 1, p256
- Zijlstra, A. A., van Hoof, P. A. M., & Perley, R. A. 2008, ApJ, 681, 1296

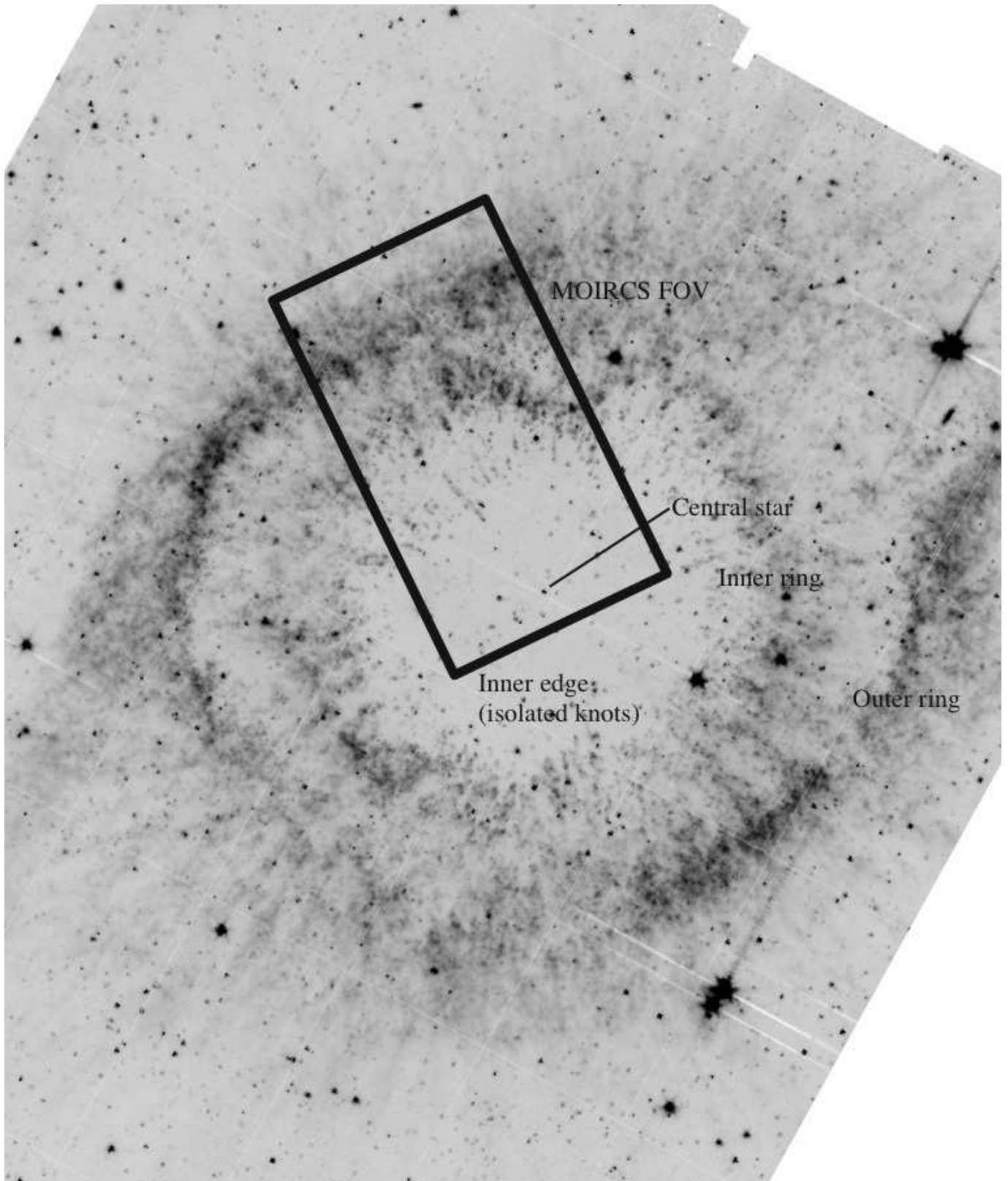


FIG. 1.— The region observed by the MOIRCS ($4' \times 7'$) is indicated by a box on the Spitzer $3.6 \mu\text{m}$ image (Hora et al. 2006). The north is top and the east is left. Two bright rings (inner and outer rings) are found in the $3.6 \mu\text{m}$ image, as well as several isolated knots in the inner edge of H_2 region. MOIRCS covers approximately one-eighth of these two rings.

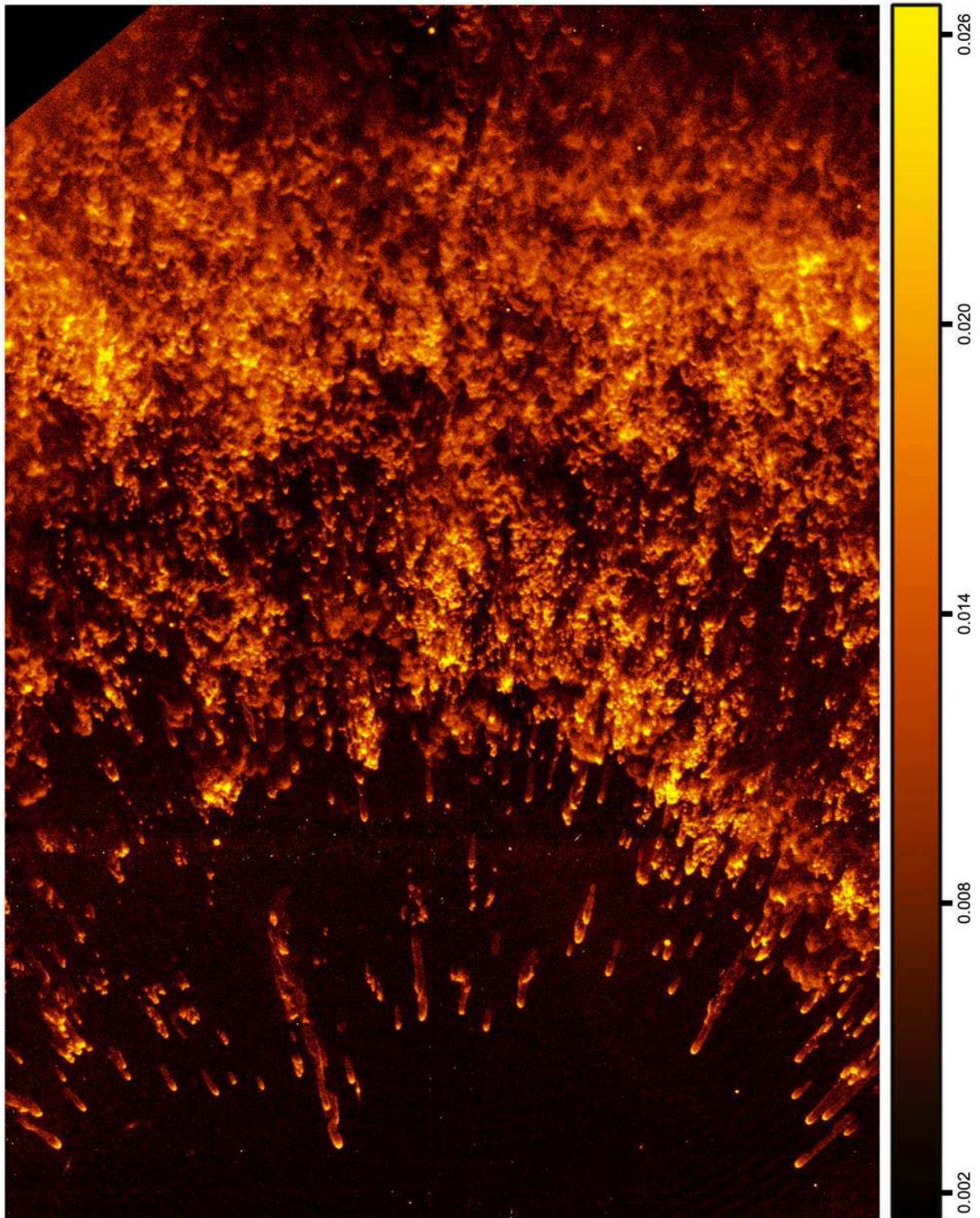


FIG. 2.— Part of the MOIRCS H₂ image covering about three-quarter ($5.10' \times 3.45'$) of the obtained image. The CS is outside of this image towards the bottom. Isolated cometary knots are found near the CS. Towards top of this figure, knots are more clustered. Here knots are not well-resolved, and rather seen as clumps. The color scale is relative intensity to the maximum counts of the image.

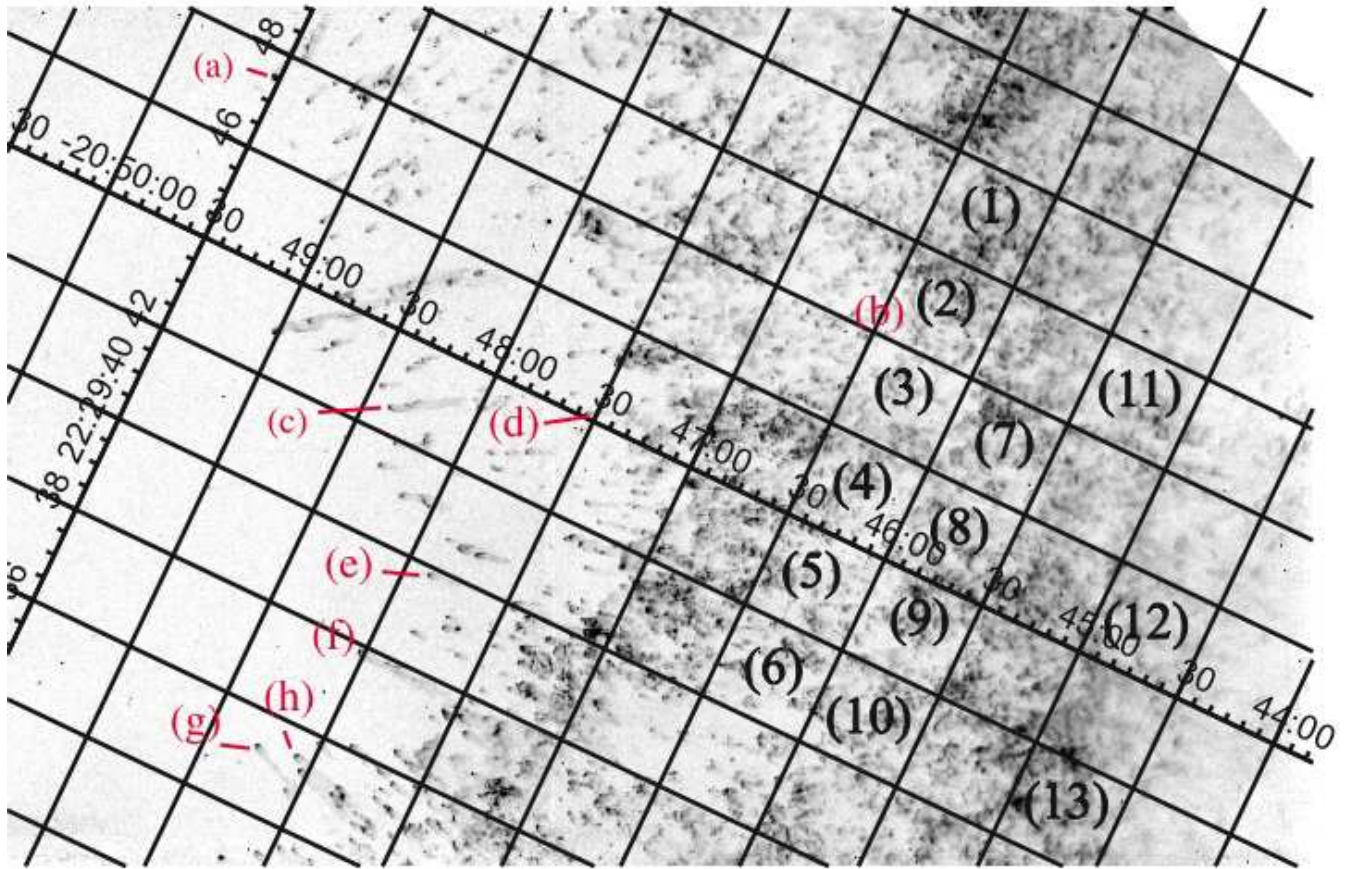


FIG. 3.— The locations where the knots enlarged in Fig. 5 are found, and where knot densities are counted, shown in close up in Fig. 4.

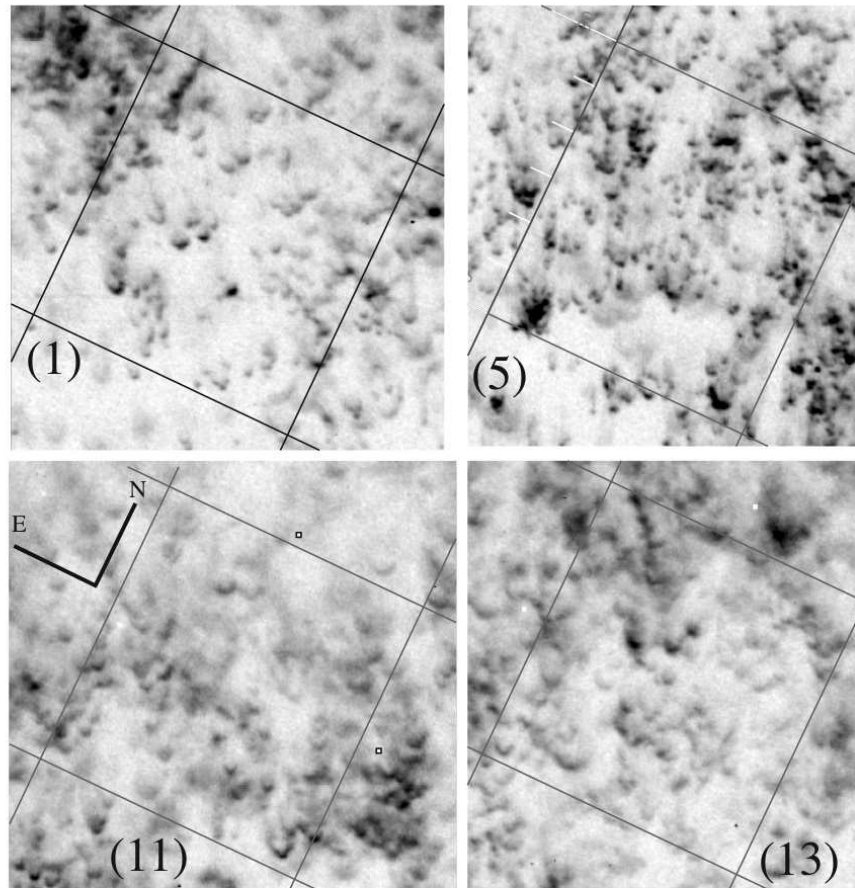
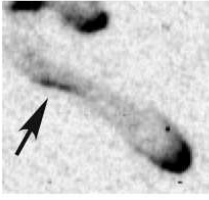


FIG. 4.— Close up of parts of the inner ring (1 & 5) and the outer ring (11 & 13) in Fig. 3, where knot densities are counted. One grid is 30'' by 30''. Clear crescent knots with tails are found in the inner ring, while fainter knots and diffuse/unresolved components are found in the outer ring.

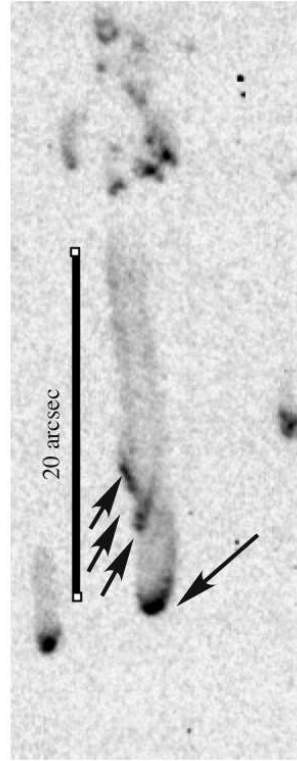
(a) 22h29m47.4s -20d49m32s
Secondary peak and meandering
Broken into two pieces?



(b) 22h29m48.7s -20d46m37s
A knot in
the outer ring



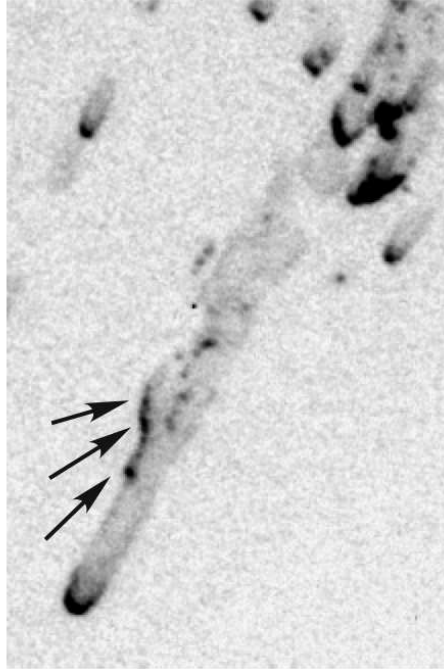
(c) 22h29m42.5s -20d48m24s
Complex (multi-peaks)



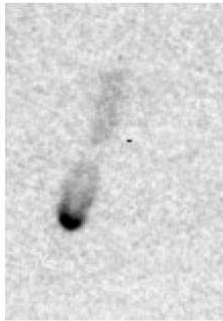
(d) 22h29m44.0s -20d47m33s
Widening after narrow



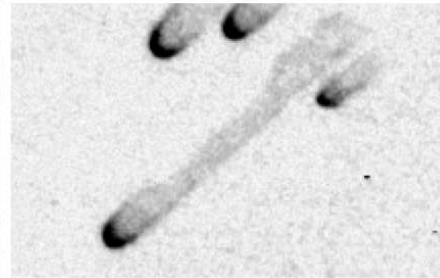
(f) 22h29m37.8s -20d48m02s
Complex (multi-peaks)



(e) 22h29m40s -20d47m53s
Narrowing
after disappearance



(h) 22h29m35.3s -20d48m16s
Widening after narrowing



(g) 22h29m35.4s -20d48m05s
Widening

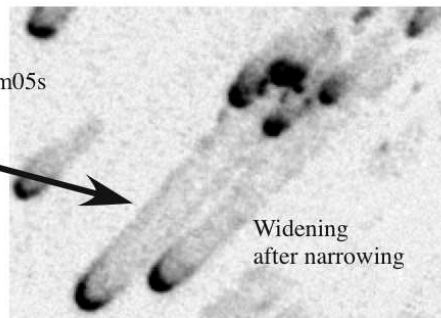


FIG. 5.— Various shapes of knots. Coordinates are in J2000. The knot (c) is identical to 44 in Meaburn et al. (1998) and (f) is identical to 1 in Meaburn et al. (1998) and 378-801 in O'Dell et al. (2005) and also found in Huggins et al. (2002) and O'Dell et al. (2007).

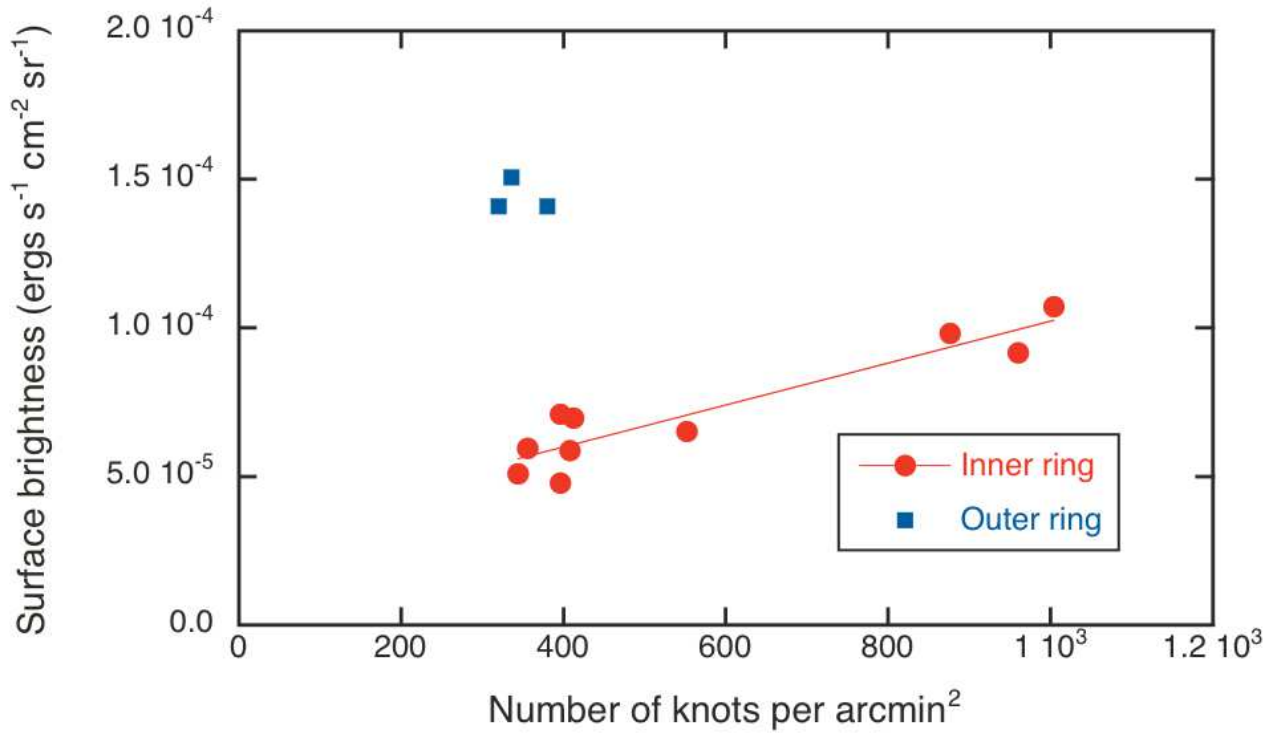


FIG. 6.— The number density of knots in $30'' \times 30''$ boxes counted in MOIRCS image, and averaged surface brightness within these boxes calculated from Speck et al. (2002). The number density of knots correlates well with the surface brightness in the inner ring. The line shows a least square fit to the data of the inner ring. The surface brightness in the outer ring is approximately twice as high as in the inner ring for a given number density of knots.

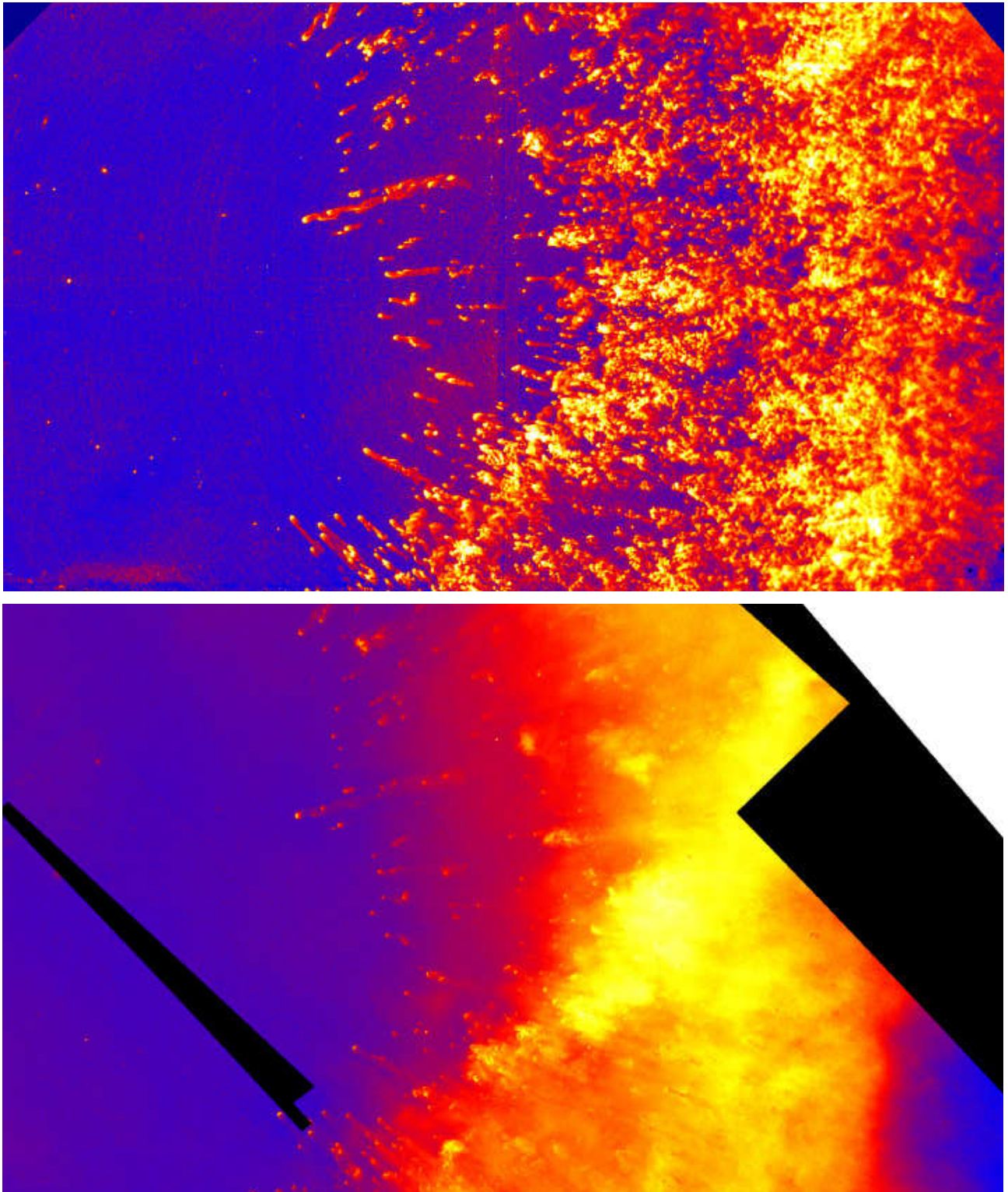


FIG. 7.— MOIRCS 7'×4' H₂ image (top) and corresponding region of the HST F658N ([NII] +Hα) image (O'Dell et al. 2004).

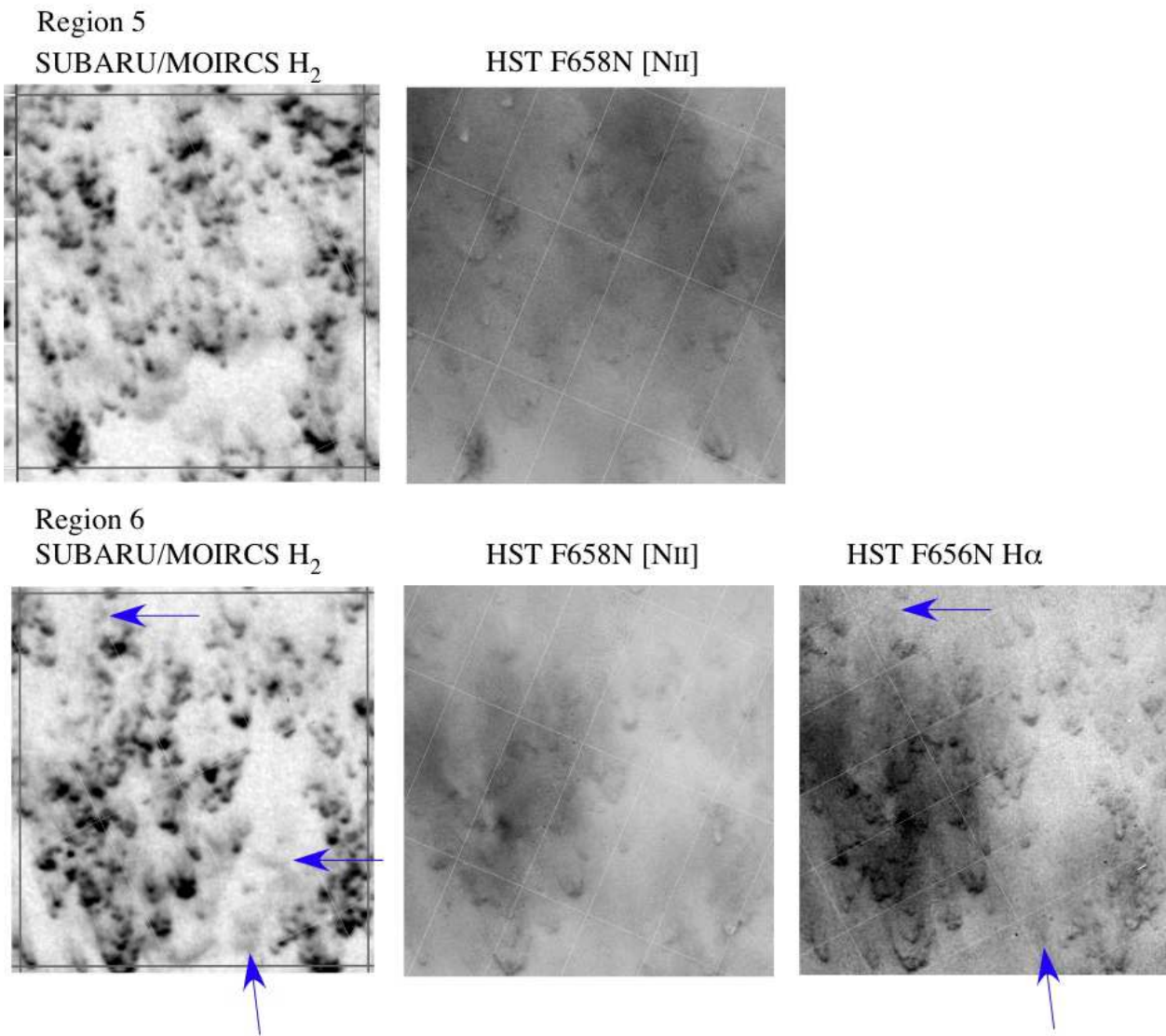


FIG. 8.— Enlarged images of regions 5 and 6 in $2.12 \mu\text{m } H_2$, F658N (658 nm; mainly [NII] with some contamination of $H\alpha$) and F656N (656 nm; $H\alpha$ with some contamination of [NII]).

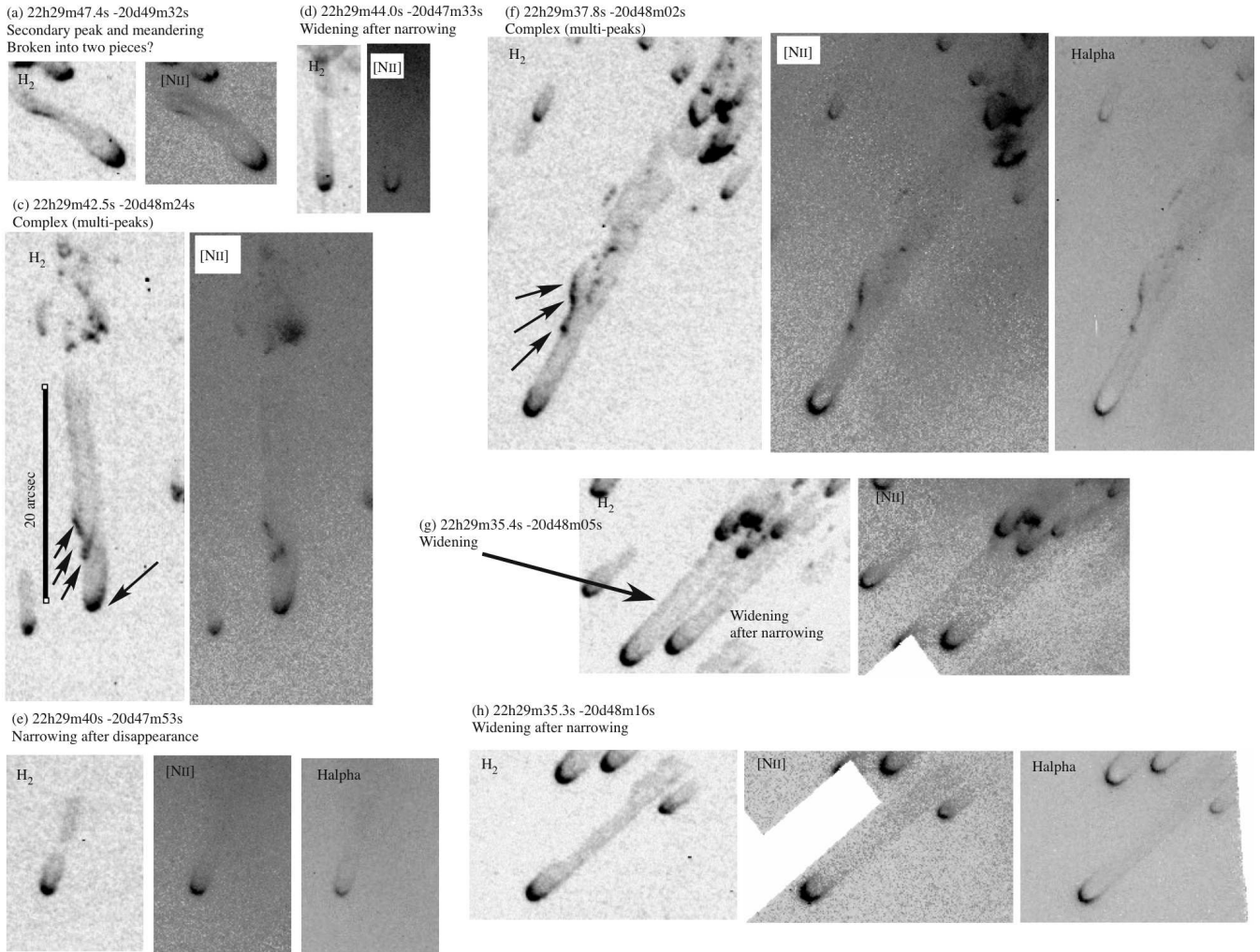


FIG. 9.— Enlarged images of knots in $2.12\ \mu\text{m}$ H_2 , F658N (658 nm; mainly $[\text{NII}]$ with some contamination of $\text{H}\alpha$) and F656N (656 nm; $\text{H}\alpha$ with some contamination of $[\text{NII}]$).